JCTC Journal of Chemical Theory and Computation

Article

Cite This: J. Chem. Theory Comput. 2019, 15, 3580−3590

pubs.acs.org/JCTC

Density Functionals from the Multiple-Radii Approach: Analysis and Recovery of the Kinetic Correlation Energy

Stefan Vuckovic*

Department of Chemistry, University of California, Irvine, California 92697, United States

ABSTRACT: Inspired by the exact form of the strongly interacting limit of density functional theory, Vuckovic and Gori-Giorgi have recently proposed [*J. Phys. Chem. Lett.* **2017**, *8*, 2799] the multiple radii functional (MRF), a new framework for the construction of exchange-correlation (xc) energy approximations able to describe strong correlation electronic effects. To facilitate the construction of improved approximations based on the MRF functional, in the present work we use reverse engineering strategies to reveal the forms of the MRF functional which reproduce the exact xc functional for small atoms. Using the adiabatic connection representation of the xc functional, we also develop an interpolation form which uses xc energy densities from the physical, weakly and strongly interacting regimes as input ingredients. We discuss how this interpolation form can be used for recovering the presently missing kinetic component of the correlation energy in the MRF framework and we asses its accuracy using highly accurate ingredients for small atoms. Applying the same interpolation form to LiH along the dissociation curve, we highlight its advantages over previous adiabatic connection-based models for the treatment of strong correlation.

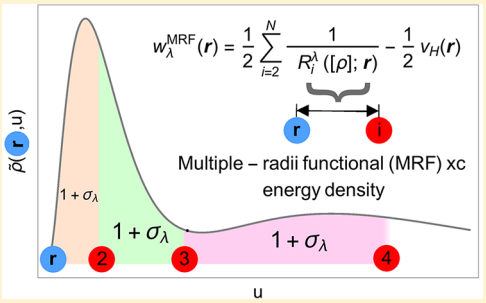

1. INTRODUCTION

With an accuracy that is often competitive with much more expensive wave function methods, Kohn−Sham Density Functional Theory (KS DFT)[1] is the most employed method in electronic structure calculations.[2−4] KS DFT is in principle an exact theory, but in practice it relies on approximations to its key quantity, the exchange-correlation (xc) functional. Mainstream strategies for the construction of density functional approximations (DFAs) to the xc functional follow the *Jacob's ladder* approach.[3,5−7] For moderately and weakly correlated systems and processes, state-of-the-art DFAs based on the Jacob's ladder approach are very close to reaching the desired chemical accuracy.[8] Despite this widespread success, accurate treatment of systems in which electronic correlation plays a prominent role (strong correlation) remains an unsolved challenge for DFAs.[2,9] This, in turn, hinders the applicability and predictive power of DFT methods due to the importance of strong correlation effects in chemical reactivity and the chemistry of transition metals.

A possible way forward for addressing the long-standing problem of strong correlation in DFT is to use the mathematics of the strongly interacting limit (SIL) of DFT as a guide for the construction of a new generation of DFAs. This limit had been proposed by Seidl[10−12] and has been carefully studied over the past decade mainly by Gori-Giorgi and co-workers.[13−16] Instead of traditional Jacob's ladder ingredients (semilocal quantities and Kohn−Sham orbitals),[5] certain integrals of the density encoding fully nonlocal information play the key role in the SIL.[10,13,14,16] Vuckovic and Gori-Giorgi have very recently constructed a whole new DFT framework by rescaling and simplifying the mathematical structure of the exact SIL. They have used integrals of the density, as the key structural motif of their framework, to reconstruct two-body quantities at the physical regime, in a way that is inspired by the exact SIL mathematics. Such an approach, named the multiple radii functional (MRF) is well-equipped for addressing long-standing problems in DFT: it is by-construction self-interaction free, and it captures the right physics of chemical bond dissociation.[17] In a physically appealing way, MRF models the pair-density in terms of *multiple effective electronic distances* or radii, which deliver the properly normalized xc hole. The MRF xc energy densities defined in terms of the xc hole also have the correct asymptotic behavior.

In the present paper we analyze several features of the MRF functional and lay the foundation for its further development. To test and explore how the proposed MRF approximation for the electron repulsion energy[17] can be improved, we reverse engineer the MRF objects to reproduce highly accurate energy densities of two-electron systems. We also use the MRF quantities that measure effective distance between electrons to analyze features of other approximate xc energy densities defined within the conventional DFT definition (the one arising from the electrostatic potential of the xc hole[18,19]). We also consider a simplification of the MRF objects that allows their reverse engineering in a way that they reproduce a given input xc energy density for systems with any electron number. This simplification also enables one to construct the MRF objects that reproduce the exact exchange energy density, and we discuss the possibility of using them to build the MRF xc functional on top of exact exchange.

Received: February 13, 2019
Published: May 13, 2019

Downloaded via VRIJE UNIV AMSTERDAM on June 17, 2020 at 21:01:27 (UTC).
See https://pubs.acs.org/sharingguidelines for options on how to legitimately share published articles.

© 2019 American Chemical Society

DOI: 10.1021/acs.jctc.9b00129
J. Chem. Theory Comput. 2019, 15, 3580−3590

Although the MRF quantities are in principle defined along the whole density-fixed adiabatic connection (AC),[20,21] so far we only have a tractable approximation to the electronic repulsion energy, a quantity that arises at the full (i.e., physical) coupling strength of the electronic interaction. For this reason, this MRF approximation misses the kinetic component of correlation energy. To start tackling this problem, in the present work, we propose a way for recovering this component by combining the information at the full coupling strength with the quantities from both weakly and strongly interacting limits by using a local interpolation along the AC. We compare this approach with other AC interpolation-based methods[11,19] and highlight its advantages over the previous efforts in this direction[22] for treating strong correlations.

2. BACKGROUND

2.1. Density-Fixed Adiabatic Connection. To give an exact expression for the xc functional, we introduce the $\Psi_\lambda[\rho]$ fermionic wave function that integrates to a given density $\rho(\mathbf{r})$ (that of a physical system) and minimizes the sum of the kinetic energy $\hat{T}$ and the electron−electron repulsion $\hat{V}_{ee}$ scaled by the non-negative coupling constant λ. By linking the Kohn−Sham (KS) noninteracting system (described by $\Psi_0[\rho] = \Phi[\rho]$) with the physical system (described by $\Psi_1[\rho]$), the exact AC expression for the xc functional is given by[20,21]

$$E_{xc}[\rho] = \int_0^1 W_\lambda[\rho]\, d\lambda \tag{1}$$

where $W_\lambda[\rho]$ is the (global) AC integrand that is given in terms of the $\Psi_\lambda[\rho]$ wave function and the Hartree energy, $U[\rho]$:

$$W_\lambda[\rho] = \langle \Psi_\lambda[\rho]|\hat{V}_{ee}|\Psi_\lambda[\rho]\rangle - U[\rho] \tag{2}$$

We can write $W_\lambda[\rho]$ as the following spatial integral over the λ dependent xc energy density, $w_\lambda(\mathbf{r})$:

$$W_\lambda[\rho] = \int w_\lambda(\mathbf{r})\rho(\mathbf{r})\, d\mathbf{r} \tag{3}$$

It is well-known in DFT that $w_\lambda(\mathbf{r})$ is not uniquely defined and several definitions (i.e., *gauges*) have been proposed for this quantity.[23,24] In the present work, we adhere to the definition of $w_\lambda(\mathbf{r})$ given in terms of the electrostatic potential of the xc hole:[18,19]

$$w_\lambda(\mathbf{r}) = \frac{1}{2}\int_0^\infty \frac{h_{xc}^\lambda(\mathbf{r}, u)}{u} 4\pi u^2\, du \tag{4}$$

where $h_{xc}^\lambda(\mathbf{r}, u)$ is the spherically averaged xc hole around $\mathbf{r}$ and arises from spherically averaged pair-, $P_2^\lambda(\mathbf{r}, u)$, and one-electron densities, $\rho_s(\mathbf{r}, u)$:

$$h_{xc}^\lambda(\mathbf{r}, u) = \frac{P_2^\lambda(\mathbf{r}, u)}{\rho(\mathbf{r})} - \rho_s(\mathbf{r}, u) \tag{5}$$

The spherically averaged pair-density, $P_2^\lambda(\mathbf{r},u)$, is obtained from $\Psi_\lambda[\rho]$:

$$P_2^\lambda(\mathbf{r}, u) = \frac{N(N-1)}{4\pi} \times \sum_{\sigma_1 \ldots \sigma_N} \int |\Psi_\lambda(\mathbf{r}\sigma_1, (\mathbf{r}+\mathbf{u})\sigma_2, \mathbf{r}_3\sigma_3, \ldots, \mathbf{r}_N\sigma_N)|^2\, d\Omega_\mathbf{u}\, d\mathbf{r}_3 \ldots d\mathbf{r}_N \tag{6}$$

while the spherically averaged density around $\mathbf{r}$ is given in terms of the following integral over the one-electron density:

$$\rho_s(\mathbf{r}, u) = \int \frac{1}{4\pi}\rho(\mathbf{r}+\mathbf{u})\, d\Omega_\mathbf{u} \tag{7}$$

The energy density in the gauge of the electrostatic potential of the xc hole (eq 4) is well-established in the literature[18,19,22,25] and for more details on the advantage of this gauge choice over the other gauges for the construction of DFAs based on eqs 1 and 3; see ref 24.

As usual, we can resolve $w_\lambda(\mathbf{r})$ into the exchange, $w_x(\mathbf{r}) = w_0(\mathbf{r})$, and the λ-dependent correlation component:

$$w_{c,\lambda}(\mathbf{r}) = w_\lambda(\mathbf{r}) - w_x(\mathbf{r}) \tag{8}$$

It is also convenient to use $w_{c,\lambda}(\mathbf{r})$ to define the λ-averaged correlation energy density, $\overline{w}_c(\mathbf{r})$:

$$\overline{w}_c(\mathbf{r}) = \int_0^1 w_{c,\lambda}(\mathbf{r})\, d\lambda \tag{9}$$

which allows us to write the correlation functional as

$$E_c[\rho] = \int \overline{w}_c(\mathbf{r})\rho(\mathbf{r})\, d\mathbf{r} \tag{10}$$

Furthermore, we can partition $\overline{w}_c(\mathbf{r})$ into its kinetic, $t_c^{hole}(\mathbf{r})$, and the electronic repulsion component, $w_{c,\lambda=1}(\mathbf{r})$:

$$\overline{w}_c(\mathbf{r}) = t_c^{hole}(\mathbf{r}) + w_{c,\lambda=1}(\mathbf{r}) \tag{11}$$

which are the local variants of $T_c[\rho] = \langle\Psi_1|\hat{T}|\Psi_1\rangle - \langle\Phi|\hat{T}|\Phi\rangle$, and $U_c[\rho] = \langle\Psi_1|\hat{V}_{ee}|\Psi_1\rangle - \langle\Phi|\hat{V}_{ee}|\Phi\rangle$, respectively. Therefore, we can write

$$E_c[\rho] = \underbrace{U_c[\rho]}_{\int w_{c,\lambda=1}(\mathbf{r})\rho(\mathbf{r})d\mathbf{r}} + \underbrace{T_c[\rho]}_{\int t_c^{hole}(\mathbf{r})\rho(\mathbf{r})d\mathbf{r}} \tag{12}$$

2.2. Mathematical Structure of the Multiple-Radii Functional. In the $\lambda \to \infty$ limit, the exact xc energy in the gauge of eq 4 has the following form:[16,26]

$$w_\infty(\mathbf{r}) = \frac{1}{2}\sum_{i=2}^N \frac{1}{|\mathbf{r} - \mathbf{f}_i([\rho]; \mathbf{r})|} - \frac{1}{2}v_h(\mathbf{r}) \tag{13}$$

where $v_h(\mathbf{r})$ is the Hartree potential and $\mathbf{f}_i([\rho]; \mathbf{r})$ are the *comotion functions*, fully nonlocal quantities that parametrize $|\Psi_\lambda|^2$ in the $\lambda \to \infty$ limit.[13,26,27] In this way, the comotion functions determine the position of the remaining $N-1$ electrons, when a reference electron is at $\mathbf{r}$. The ultra nonlocality of comotion functions makes their evaluation highly complex and for general 3D geometries they have been obtained only for systems with few electrons.[16,28,29] From eq 13, we can see that a distance between a reference electron and the remaining $N-1$ electrons fully determines the xc energy density in the strong coupling limit. The idea of the *multiple-radii functional* of Vuckovic and Gori-Giorgi is based on the generalization of eq 13 along the adiabatic connection. They defined the MRF energy densities along the AC in terms of the λ-dependent *effective electronic distances* or radii:

$$w_\lambda^{MRF}(\mathbf{r}) = \frac{1}{2}\sum_{i=2}^N \frac{1}{R_i^\lambda([\rho]; \mathbf{r})} - \frac{1}{2}v_H(\mathbf{r}) \tag{14}$$

The associated MRF spherically averaged pair-density, which gives rise to eq 14, is given by

$$P_{2,\lambda}^{MRF}([\rho]; \mathbf{r}, u) = \frac{1}{4\pi u^2}\sum_{i=2}^N \rho(\mathbf{r})\delta(u - R_i^\lambda(\mathbf{r})) \tag{15}$$

DOI: 10.1021/acs.jctc.9b00129
J. Chem. Theory Comput. 2019, 15, 3580−3590

with δ being the Dirac delta function. As $P^{\mathrm{MRF}}_{2,\lambda}([\rho];\,\mathbf{r},\,u)$ is given by the sum of the δ functions, it does not resemble the exact pair-density at finite λ. For this reason, the MRF pair density is a fictitious object whose purpose is to reproduce the $w_\lambda(\mathbf{r})$ xc energy density, which is the quantity that we aim to approximate within the MRF framework. Along these lines, it has been shown that the corresponding $w_1^{\mathrm{MRF}}(\mathbf{r})$ of eq 14 represents an accurate approximation to its exact counterpart.[17]

The MRF framework uses the full, yet computationally tractable, nonlocality inspired by the exact forms of the comotion functions. This nonlocality is built from the following integrals over the spherically averaged density of eq 7:

$$N_e(\mathbf{r},\,u) = \int_0^u 4\pi x^2 \rho_s(\mathbf{r},\,x)\,\mathrm{d}x \tag{16}$$

The crucial physical quantity, defined in terms of $N_e(\mathbf{r},\,u)$ that has been used for studying and defining the $R_i^\lambda([\rho];\,\mathbf{r})$ radii:

$$\nu_i^\lambda(\mathbf{r}) = N_e(\mathbf{r},\,R_i^\lambda(\mathbf{r})), \qquad i = 2,\,...,\,N \tag{17}$$

gives the expected number of electrons inside of a sphere centered at $\mathbf{r}$ and having radius $R_i^\lambda(\mathbf{r})$.

In ref 17, an approximation to the xc energy densities at the physical coupling strength has been constructed from the physical argument by expecting that $\nu_2^{\lambda=1}(\mathbf{r}) \approx 1$, $\nu_3^{\lambda=1}(\mathbf{r}) \approx 2$, ..., $\nu_N^{\lambda=1}(\mathbf{r}) \approx N-1$. We can thus write the $\nu_i^\lambda(\mathbf{r})$ along the AC as

$$\nu_i^\lambda(\mathbf{r}) = i - 1 + \sigma_i^\lambda(\mathbf{r}), \qquad i = 2,\,...,\,N \tag{18}$$

where $\sigma_i^\lambda(\mathbf{r})$ is the *fluctuation function*, which can push away or bring closer the ith electron to the reference electron, with respect to the expected distance at $\lambda = 1$: $a_i(\mathbf{r}) = N_e^{-1}(\mathbf{r},\,i-1)$. In the same ref 17, a simple ansatz inspired by the exact mathematical feature of SIL[13,17] $\sigma_i^{\lambda=1}(\mathbf{r})$ has been used:

$$\sigma_i^{\lambda=1}(\mathbf{r}) = \frac{1}{2}\mathrm{e}^{-bS_i(\mathbf{r})^2} \tag{19}$$

where $b = 5$ has been chosen to optimize $W_1[\rho]$ for the helium atom and where $S_i(\mathbf{r})$:

$$\begin{aligned} S_i(\mathbf{r}) &= \frac{\partial N_e(\mathbf{r},\,u)}{\partial u}\Big|_{u=N_e^{-1}(\mathbf{r},i-1)} \\ &= 4\pi a_i(\mathbf{r})^2 \tilde{\rho}(\mathbf{r},\,a_i(\mathbf{r})) \end{aligned} \tag{20}$$

gives the information on the radial spherically averaged density of the i-th neighboring electron. Combining eqs 3, 14, 17, and 18, we finally arrive at

$$W_\lambda^{\mathrm{MRF}}(\mathbf{r}) = \frac{1}{2}\int \mathrm{d}\mathbf{r}\,\rho(\mathbf{r}) \sum_{i=2}^{N} \frac{1}{N_e^{-1}(\mathbf{r},\,\underbrace{i-1+\sigma_i^\lambda(\mathbf{r})}_{\nu_i^\lambda(\mathbf{r})})} - U[\rho] \tag{21}$$

Equation 21 shows that within the MRF functional, the problem of the construction of the AC integrand (and thus also approximate $E_{\mathrm{xc}}[\rho]$) is reduced to the construction of the $\sigma_i^\lambda(\mathbf{r})$ fluctuation functions in terms of $S_i(\mathbf{r})$ of eq 20. Note that even a primitive ansatz for $\sigma_i^\lambda(\mathbf{r})$, as that of eq 19, yields rather accurate energy densities at the full coupling strength. The main object of the following sections is to use highly accurate energy densities to obtain "exact" $\sigma_i^\lambda(\mathbf{r})$ to challenge the ansatz of eq 19. Note that by the exact σ_i^λ we refer to the one which reproduces the corresponding exact $w_\lambda(\mathbf{r})$.

3. MRF FUNCTIONAL FOR TWO-ELECTRON SYSTEMS

3.1. MRF Objects from Exact xc Energy Densities. To gain more insight into how approximations from the MRF framework can be improved, we first consider two-electron systems. In the case of two-electron systems, there is only one radius appearing in eq 14, and this allows us to invert eq 14 to obtain this radius in terms of the xc energy density and the Hartree potential:

$$R_2^\lambda(\mathbf{r}) = \frac{1}{v_H(\mathbf{r}) + 2w_\lambda(\mathbf{r})} \qquad (N=2) \tag{22}$$

From highly accurate $w_\lambda(\mathbf{r})$ energy densities of two-electron systems, we can use eq 22 to obtain the "exact" $R_2^\lambda(\mathbf{r})$. We observe here the trends in the MRF quantities across the helium isolectronic series. Since a reasonable approximation for the density of this series is given by[30]

$$\rho_Z(\mathbf{r}) \approx Z^3\rho(Z\mathbf{r}) \tag{23}$$

we can observe how the key MRF objects change, as the density becomes more compact with the increase of the nuclear charge Z. As said, by plugging the exact energy density into eq 22, we can directly obtain the "exact" $R_2^\lambda(\mathbf{r})$. However, it is more interesting to calculate the corresponding $\nu^\lambda(\mathbf{r})$ and $\sigma^\lambda(\mathbf{r})$ quantities, as the two quantities are expected to be more universal, in the sense that we expect them to be less system- and $\mathbf{r}$-dependent (see eqs 17 and 18). Combining eqs 17, 18, 22, we can write $\sigma_2^\lambda(\mathbf{r})$ as

$$\sigma_2^\lambda(\mathbf{r}) = \underbrace{N_e(\mathbf{r},\,(v_H(\mathbf{r}) + 2w_\lambda(\mathbf{r}))^{-1})}_{\nu_2^\lambda(\mathbf{r})} - 1 \tag{24}$$

In Figure 1, we show the "exact" $\sigma^\lambda(\mathbf{r}) = \sigma_2^\lambda(\mathbf{r})$ quantities for the members of the helium isoelectronic series with Z values from 1 to 10, at $\lambda = 0$ (upper panel) and at $\lambda = 1$ (lower panel). The $\sigma^1(\mathbf{r})$ curves have been obtained from eq 24 by using highly accurate $w_\lambda(\mathbf{r})$ energy densities at the full coupling strength. The wave function at the full coupling strength, used for calculating $w_1(\mathbf{r})$ (eq 4), has been obtained from the GAMESS-US package[31] at the full-CI level within the aug-cc-pVQZ basis set.[32] The one-electron density from this wave function has been used for obtaining $w_0(\mathbf{r})$, since for $N = 2$ it can be calculated from the Hartree potential: $w_0(\mathbf{r}) = -(4v_h(\mathbf{r}))^{-1}$.

To understand the trend in the exchange ($\lambda = 0$) $\sigma^\lambda(\mathbf{r})$ curves, as Z is varied, we note that eq 23 dictates the following scaling of the exchange energy density:

$$w_x([\rho_Z];\,\mathbf{r}) = \frac{1}{Z}w_x\left([\rho];\,\frac{\mathbf{r}}{Z}\right) \tag{25}$$

Equation 25, in turn, dictates the following scaling of $\sigma^0(\mathbf{r})$ for the helium isoelectronic series:

$$\sigma^0([\rho_Z];\,\mathbf{r}) = \sigma^0([\rho];\,Z\mathbf{r}) \tag{26}$$

Equation 26 explains why the exchange $\sigma^0(\mathbf{r})$ curves, shown in the upper panel Figure 1, do not change substantially as Z is varied. In fact, they would be all the same, if the density of the helium isolectronic series satisfies exactly eq 23.

We move now to the $\sigma^1(\mathbf{r})$ curves, shown in the lower panel of Figure 1. We can see that starting from the hydride ion,

DOI: 10.1021/acs.jctc.9b00129
J. Chem. Theory Comput. 2019, 15, 3580−3590

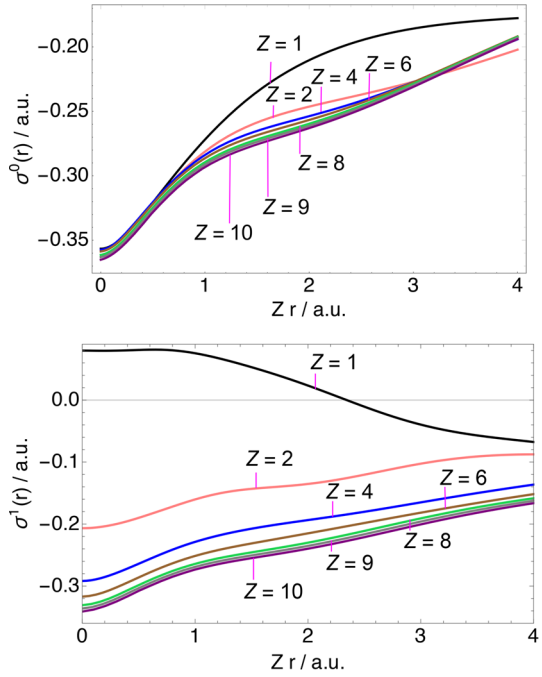

Figure 1. Plots of $\sigma^0(\mathbf{r})$ (upper panel) and $\sigma^1(\mathbf{r})$ (lower panel) quantities of eq 24 for the helium isoelectronic series with nuclear charges $1 \leq Z \leq 10$ and with radial distance r/a.u. scaled by nuclear charge.

$\sigma^1(\mathbf{r}) \approx 0$, $\sigma^1(\mathbf{r})$ decreases with Z and then quickly scales to an asymptotic constant that lies around −0.3. By analogy with eq 8, we define the correlation component of $\sigma_\lambda(\mathbf{r})$ as

$$\sigma_i^{c,\lambda}(\mathbf{r}) = \sigma_i^{\lambda}(\mathbf{r}) - \sigma_i^{0}(\mathbf{r}) \tag{27}$$

We can observe from Figure 1 that $\sigma^{c,1}(\mathbf{r})$ (i.e., the difference between $\sigma^1(\mathbf{r})$ and $\sigma^0(\mathbf{r})$) decreases with Z. At large Z, it scales to a small positive constant $\sigma_i^{c,1}(\mathbf{r}) \approx 0.04$, reflecting that in the high-density limit (at least for nondegenerate KS systems) correlation becomes just a small perturbation.[33,34]

We can see now that the present MRF approximation to $w_1(\mathbf{r})$ of eq 19, constructed based on physical arguments,[17] is not flexible enough to capture the $\sigma^1(\mathbf{r})$ curves at larger Z values of Figure 1. This is because the approximate $\sigma^1(\mathbf{r})$ of eq 19 is bounded by 0 from below. The results of this section can already be used for improving the form $\sigma_2^1(\mathbf{r})$ of eq 19, by allowing it to be negative in high-density regimes. More specifically, $\sigma_2^1(\mathbf{r})$ can be improved by allowing it to go to ∼ −0.3, instead of 0, as the high-density limit, signaled by large $S_2(\mathbf{r})$ values, is approached. Alternatively, if one wants to approximate $\sigma_i^{c,1}(\mathbf{r})$ on top of exact exchange (this route will be discussed in Section 4), one can ensure that $\sigma_i^{c,1}(\mathbf{r})$ goes to a small positive constant, as the high-density limit, again signaled by large $S_2(\mathbf{r})$, is approached.

3.2. MRF Objects from Approximate Energy Densities. In addition to the exact $\sigma^\lambda(\mathbf{r})$ for $N = 2$ shown in Section 3.1, we can also compute $\sigma^\lambda(\mathbf{r})$ from DFAs by plugging approximate $w_\lambda(\mathbf{r})$ into eq 24. To have a meaningful comparison of the exact and approximate $\sigma^\lambda(\mathbf{r})$, we remark again that the approximate $w_\lambda(\mathbf{r})$, entering eq 24, also needs to be in the gauge of eq 4. We employ here the local density approximation (LDA)[1] for obtaining approximate $\sigma^\lambda(\mathbf{r})$ at $\lambda = 0$ and $\lambda = 1$, as well as the Becke-Roussel (BR) model[35] for the energy density at $\lambda = 0$. Note that other DFAs, such as common (meta)-GGAs, typically do not model $w_\lambda(\mathbf{r})$ defined by eq 4.[19,36]

In Figure 2 we compare the exact $\sigma^1(\mathbf{r})$ with that from the LDA functional for the helium atom and the hydride ion. In

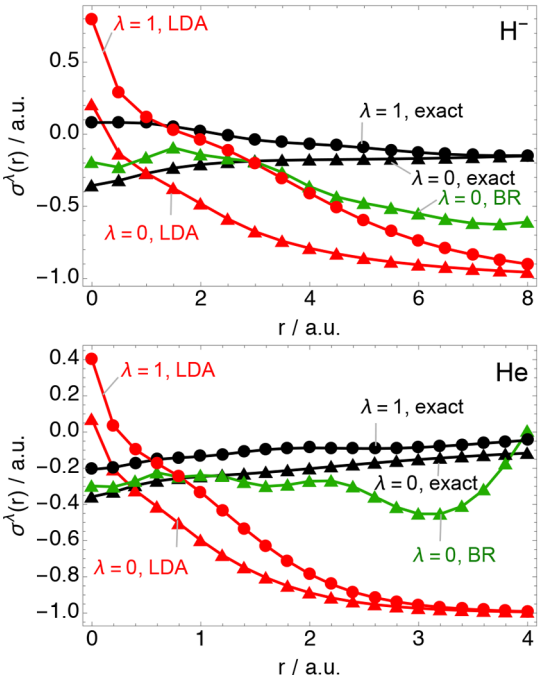

Figure 2. Plots of the exact and approximate $\sigma^\lambda(r)$ quantities of eq 24 for the hydride ion (upper panel) and the helium atom (lower panel), at $\lambda = 0$ (triangles) and $\lambda = 1$ (circles).

the same figure we also compare the exchange $\sigma^0(\mathbf{r})$ quantity with the approximate ones from the BR and LDA exchange energy densities. The expressions used for evaluating the LDA and BR energy densities and further computational details are given in Appendix A. We can see from Figure 2 that the exact $\sigma^1(\mathbf{r})$ stays nearly constant: $\sigma^1(\mathbf{r}) \approx 0$ for H^- and $\sigma^1(\mathbf{r}) \approx -0.1$ for He. Contrary to the exact $\sigma^\lambda(\mathbf{r})$, at both $\lambda = 0$ and $\lambda = 1$, those of LDA substantially change with $\mathbf{r}$: they are too large when a reference electron is close to the nucleus and then at large r they tend to −1. This mirrors the fact that the magnitude of the LDA xc energy is strongly overestimated in the region around a nucleus, while in valence atomic regions it is underestimated.[37,38]

Given that for two-electron systems $R_2^\lambda(\mathbf{r})$ represents the effective distance between electrons, the $\nu^\lambda(\mathbf{r}) = \sigma^\lambda(\mathbf{r}) + 1$ quantity represents *the charge associated with the effective distance between electrons* (see eqs 17, 18, and 24). We can also see from Figure 2 that $\sigma^0(\mathbf{r})$ and $\sigma^1(\mathbf{r})$ of LDA unphysically tend to −1 at large $\mathbf{r}$, and in this way the corresponding LDA $\nu^\lambda(\mathbf{r})$ charges tend to 0 at large $\mathbf{r}$. We can understand this unphysical behavior of LDA in the light of the features of the underlying xc holes. When a reference electron is placed in the atomic tail, where the density is very low, the LDA xc hole becomes very shallow. This makes the magnitude of electrostatic potential of the LDA xc hole very small (i.e., the w^{LDA} xc energy density) and it decays exponentially, instead of $\sim -\frac{1}{2|\mathbf{r}|}$ at large $\mathbf{r}$. For this reason, the underlying LDA $\nu^0(\mathbf{r})$ and $\nu^1(\mathbf{r})$ charges drop to 0 at large $\mathbf{r}$.

From Figure 2, we can see that although the $\sigma^0(\mathbf{r})$ of the BR approximation is still not in quantitative agreement with the

DOI: 10.1021/acs.jctc.9b00129
J. Chem. Theory Comput. 2019, 15, 3580−3590

exact $\sigma^0(\mathbf{r})$, it displays a large improvement over the LDA, particularly in the region near the nucleus. The improvement $\sigma^0(\mathbf{r})$ of BR over that of LDA is also noticeable in the valence region. This is what one would expect, since $w_0^{\mathrm{BR}}(\mathbf{r})$ by construction has the correct $\sim -\frac{1}{2|\mathbf{r}|}$ asymptotic behavior for $|\mathbf{r}| \to \infty$.[35]

4. REVERSE MRF MACHINERY

One of the key advantages of the MRF framework for building new DFAs is its full, yet computationally tractable, nonlocality. It is well-known that, if we want to use the exact exchange energy density, we need fully nonlocal correlation to be compatible with it.[39−41] To obtain a starting point for the construction of the MRF correlation functional on top of exact exchange, we can think of engineering $\sigma_i^x(\mathbf{r})$ quantities, which reproduces the exact exchange energy density $w_x(\mathbf{r})$. Note that a similar strategy has already been explored and used in the construction of DFAs, such as the *reverse Becke−Roussel machinery*, where a model exchange hole is engineered in such a way to reproduce the exact $w_x(\mathbf{r})$.[42−44]

More generally, to pursue the idea of reverse engineering $\sigma_i^\lambda(\mathbf{r})$ that reproduces given $w_\lambda(\mathbf{r})$, we first rewrite eq 14 as

$$\sum_{i=2}^{N} R_i^\lambda([\rho];\mathbf{r}) = \frac{1}{v_H(\mathbf{r}) + 2w_\lambda(\mathbf{r})} \tag{28}$$

By plugging eq 17 into eq 28, we can write

$$\sum_{i=2}^{N} N_e^{-1}(\mathbf{r}, i-1+\sigma_i^\lambda(\mathbf{r})) = \frac{1}{v_H(\mathbf{r}) + 2w_\lambda(\mathbf{r})} \tag{29}$$

For systems with $N > 2$ we cannot find a unique set of $(\sigma_2^\lambda(\mathbf{r}), \ldots, \sigma_N^\lambda(\mathbf{r}))$ that yields the input energy density $w_\lambda(\mathbf{r})$. To circumvent this problem, we consider a simplification by i-averaging the fluctuation function of eq 18: $\sigma_i^\lambda(\mathbf{r}) \approx \tilde{\sigma}^\lambda(\mathbf{r})$. With this simplification, eq 29 becomes

$$\sum_{i=2}^{N} N_e^{-1}(\mathbf{r}, i-1+\tilde{\sigma}^\lambda(\mathbf{r})) = \frac{1}{v_H(\mathbf{r}) + 2w_\lambda(\mathbf{r})} \tag{30}$$

Equation 30 now ensures that for a given density there is a one-to-one correspondence between $\tilde{\sigma}^\lambda(\mathbf{r})$ and $w_\lambda(\mathbf{r})$, allowing us to reverse engineer $\tilde{\sigma}^\lambda(\mathbf{r})$ by using the $w_\lambda(\mathbf{r})$ input energy density. Another appealing feature of eq 30 is that $w_\lambda(\mathbf{r})$ always decreases (becomes more negative) as $\tilde{\sigma}^\lambda(\mathbf{r})$ increases. This simply arises from eq 16, as $N_e(\mathbf{r},u)$ increases with u, given that $\rho_s(\mathbf{r},u) \geq 0$.

The primary use of eq 30 would be to obtain $\tilde{\sigma}^x(\mathbf{r})$ that reproduces the exact exchange energy density, $w_x(\mathbf{r})$. As discussed in section 2.2, the λ-dependent fluctuation function, $\sigma_i^\lambda(\mathbf{r})$, defines the MRF xc functional by means of eqs 21 and 1. Setting

$$\sigma_i^\lambda(\mathbf{r}) = \tilde{\sigma}^x(\mathbf{r}) + \sigma_i^{c,\lambda}(\mathbf{r}) \tag{31}$$

where $\sigma_i^{c,0}(\mathbf{r}) = 0$, we ensure that the MRF functional is built on top of exact exchange. At the same time, we obtain a starting point for the construction of $\sigma_i^\lambda(\mathbf{r})$ and the idea is to build $\sigma_i^{c,\lambda}(\mathbf{r})$ using simple $S_i(\mathbf{r})$ -dependent forms, akin to eq 19. Note again that xc functional approximations based on eq 31 would use $w_x(\mathbf{r})$ as an input ingredient, as this quantity is needed for obtaining $\tilde{\sigma}^x(\mathbf{r})$ by means of eq 30. The dependence of $\sigma_i^\lambda(\mathbf{r})$ on λ will be discussed in the remainder of this section.

Along the lines of the $\sigma_i^\lambda(\mathbf{r})$ dependence on λ, as discussed in section 2.2, we expect $\sigma_i^1(\mathbf{r})$ on average to be around 0. The MRF functional based on this assumption (more precisely with the fluctuation function of eq 19, which keeps $\sigma_i^1(\mathbf{r})$ close to 0, unless the corresponding $S_i(\mathbf{r})$ becomes very small) yields rather accurate $W_1^{\mathrm{MRF}}[\rho]$ values.[17] Even though the corresponding $w_1^{\mathrm{MRF}}(\mathbf{r})$ is overall rather accurate as well, it has a deficiency that it does not always satisfy the $w_1^{\mathrm{MRF}}(\mathbf{r}) \leq w_x(\mathbf{r})$ inequality. For example, we have observed that in intershell atomic regions (already in the case of the neon atom that will be discussed below), $w_1^{\mathrm{MRF}}(\mathbf{r})$ unphysically lies above the exact $w_x(\mathbf{r})$. This can be particularly problematic if $w_1^{\mathrm{MRF}}(\mathbf{r})$ is used for the construction of the correlation functional by means of an AC-based interpolation between the xc energy densities at $\lambda = 0$ and $\lambda = 1$ (this route will be explored in section 5). On the positive side, this deficiency can be easily fixed by defining a constraint based on the $\tilde{\sigma}^x(\mathbf{r})$ fluctuation function, which, as said, can be obtained by inversion from the exact energy density (eq 30). More specifically, by simply constraining $\sigma_i^1(\mathbf{r})$ to satisfy

$$\sigma_i^1(\mathbf{r}) \geq \tilde{\sigma}^x(\mathbf{r}) \tag{32}$$

or equivalently $\sigma_i^{c,\lambda}(\mathbf{r}) \geq 0$, we ensure that the corresponding $w_1^{\mathrm{MRF}}(\mathbf{r})$ always lies below the exact exchange energy density (i.e $w_{c,1}^{\mathrm{MRF}}(\mathbf{r}) = w_1^{\mathrm{MRF}}(\mathbf{r}) - w_x(\mathbf{r}) \leq 0$).

Besides using eq 30 to obtain the "exact" $\tilde{\sigma}^x(\mathbf{r})$, we can calculate exact $\tilde{\sigma}^\lambda(\mathbf{r})$ for other λ values. These quantities can be used as a guide for the construction of the λ-dependent fluctuation functions (see eq 21). Thus, in Figure 3, we show

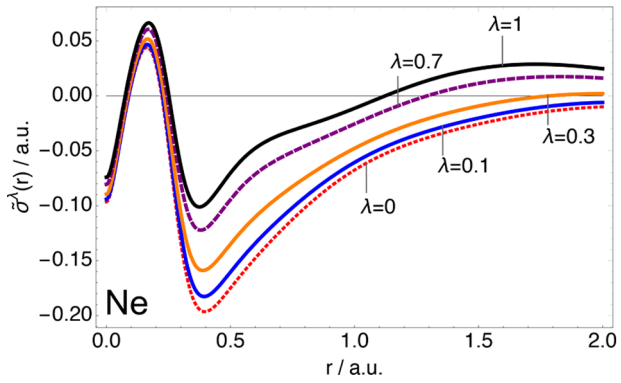

Figure 3. $\tilde{\sigma}^\lambda(r)$ quantity of eq 30 along the AC for the neon atom delivering the exact xc energy densities in the gauge of eq 4, with $0 \leq \lambda \leq 1$.

$\tilde{\sigma}^\lambda(\mathbf{r})$ for the neon atom for several λ values between 0 and 1 calculated from highly accurate $w_\lambda(\mathbf{r})$ energy densities. The highly accurate energy densities used throughout this section have been taken from refs 19, 22, and 45. They have been obtained from the $\Psi_\lambda[\rho]$ at the CCSD[46]/aug-cc-pCVTZ[32] level of theory. The CCSD method has been used in combination with the Lieb maximization algorithm of Teale and co-workers to constrain Ψ_λ to always integrate to the physical $\rho(\mathbf{r})$ (i.e., that at $\lambda = 1$). For more details on this methodology, see refs 19, 30, 47, and 48.

From Figure 3, we can see that $\tilde{\sigma}^\lambda(\mathbf{r})$ curves at $\lambda > 0$ essentially follow the shape of $\tilde{\sigma}^0(\mathbf{r})$, and they become more positive with the increase of λ, mirroring that as λ increases electrons are effectively further from one another. This again illustrates a neat property of MRF that $w(\mathbf{r})$ always decreases

DOI: 10.1021/acs.jctc.9b00129
J. Chem. Theory Comput. 2019, 15, 3580−3590

with $\tilde{\sigma}(\mathbf{r})$ (eq 30). Interestingly, we can also see from Figure 3 that in the intershell region ($r \sim 0.3$ au) the $\tilde{\sigma}^0(r) = \tilde{\sigma}^x(r)$ quantity is above 0. Given that in this region $\sigma_i^1(r)$ of eq 19 is very close to 0, the corresponding $w_1^{MRF}(r)$ will incorrectly lie above the exact $w_0(r)$. In intershell atomic regions the total xc effects are strongly dominated by exchange,[49] and in this case, the exchange itself is *more efficient in keeping electrons away from one another* than the MRF model for $\lambda = 1$ pertinent to eq 19. As discussed earlier in this section, this problem can be fixed by building $\sigma_i^1(\mathbf{r})$ models that satisfy eq 32.

Another interesting feature of the MRF functional based on the fluctuation function of eq 19 is that for neutral atoms its accuracy increases with N.[17] For example, it gives the following relative errors in $W_1[\rho]$ energies: 7.4% for He and −1% for Be, whereas for Ne and Ar it drops to 0.5% and −0.5%, respectively. To try to better understand this observation, in Figure 4, we show the $\sigma_i^1(\mathbf{r})$ evaluated on the highly accurate

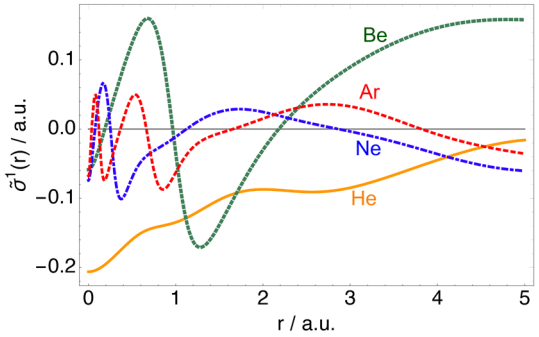

Figure 4. $\tilde{\sigma}^1(r)$ quantity of eq 30 at the full coupling strength for the helium, beryllium, neon, and argon atoms.

$w_1(\mathbf{r})$ (the computational details are the same as those of Figure 3) for the four atoms. We can observe that as we go from He, over Be to Ne/Ar, the exact $\tilde{\sigma}^1(\mathbf{r})$ is getting closer to 0. This indeed rationalizes the observed trend in accuracy of $W_1^{MRF}[\rho]$, given that $\sigma_i^1(\mathbf{r}) \geq 0$ of eq 19 stays very close to 0 for neutral atoms.

5. RECOVERING THE KINETIC COMPONENT OF THE CORRELATION ENERGY VIA INTERPOLATION ALONG THE ADIABATIC CONNECTION

From eqs 21 and 1, we can see that the λ-dependent fluctuation functions for λ values between 0 and 1 completely define the MRF xc functional. Having a simple form, akin to eq 19, for the λ-dependent fluctuation functions, which produce accurate xc energy values, is indeed the ultimate goal concerning the construction of the MRF xc functional. However, given that so far it has been shown that only accurate $W_\lambda^{MRF}[\rho]$ and $w_\lambda^{MRF}(\mathbf{r})$ quantities at $\lambda = 1$ have been constructed, in this section we consider the possibility of recovering the $E_{xc}[\rho]$ functional by combining quantities at $\lambda = 1$ with quantities from the weakly and strongly interacting limits. Note that by having only the $\lambda = 1$ point of the AC connection (without the full dependence between 0 and 1), we miss the kinetic component of $E_{xc}[\rho]$, given that the xc functional can also be written as

$$E_{xc}[\rho] = W_1[\rho] + T_c[\rho] \tag{33}$$

In this section we develop a method based on a local interpolation along the adiabatic connection to recover $T_c[\rho]$ by using the xc energy density at the full coupling strength as one of the input quantities for the interpolation. We remark that this approach is very general and thus not useful only for the MRF functional but also for other approaches that have a model for $w_1(\mathbf{r})$. These include the $w_1(\mathbf{r})$ model pertinent to the B13 functional[44,50] but also correlation factor approaches, where for example a correlation factor can be designed to transform the exact $h_x^{\lambda=0}(\mathbf{r}, u)$ into $h_{xc}^{\lambda=1}(\mathbf{r}, u)$.[51,52] We remark that similar AC-based approaches for the construction of $E_{xc}[\rho]$ approximations have been already considered,[19,22,53−55] and in what follows we will briefly review these approaches and describe how they will be adjusted to include the $\lambda = 1$ information in the interpolation scheme.

Interpolations along the adiabatic connection between the weak and strong coupling limit of DFT have been utilized by Seidl and co-workers for the construction of the interaction strength interpolation (ISI) family of the xc functional approximations.[11,12,14,56] The major problem with the ISI framework is its lack of size-consistency,[57,58] which can be remedied by a simple correction that works for systems that dissociate into fragments with nondegenerate ground states.[59] Size-consistency of the ISI framework can also be recovered if one does a local, instead of a global, interpolation along the AC (i.e., at each point in space) by using the energy densities of eq 4.[19,22,54,55] One of the simplest ISI interpolation forms that has been used for both global and local AC interpolation is the SPL (after Seidl, Perdew, and Levy) form:[11,13,19]

$$w_\lambda^{SPL}(\mathbf{r}) = a(\mathbf{r}) + \frac{b(\mathbf{r})}{\sqrt{1 + c(\mathbf{r})\lambda}} \tag{34}$$

The three parameters of eq 34 are fixed by the ingredients used in the SPL interpolation scheme, $\mathbf{w}_{SPL}(\mathbf{r}) = \{w_0, w_0', w_\infty\}$, and they are given by

$$\begin{aligned} a^{SPL}(\mathbf{r}) &= w_\infty(\mathbf{r}) \\ b^{SPL}(\mathbf{r}) &= w_0(\mathbf{r}) - w_\infty(\mathbf{r}) \\ c^{SPL}(\mathbf{r}) &= -\frac{2w_0'(\mathbf{r})}{w_0(\mathbf{r}) - w_\infty(\mathbf{r})} \end{aligned} \tag{35}$$

With small adjustments, we can still use the SPL form by replacing $w_0'(\mathbf{r})$ of $\mathbf{w}_{SPL}(\mathbf{r})$ with the energy density at the full-coupling strength, $w_1(\mathbf{r})$. We denote this interpolation form by SPL1, and its input ingredients are $\mathbf{w}_{SPL1}(\mathbf{r}) = \{w_0, w_1, w_\infty\}$. These ingredients now fix the SPL1 parameters entering eq 34:

$$\begin{aligned} a^{SPL1}(\mathbf{r}) &= a^{SPL}(\mathbf{r}) \\ b^{SPL1}(\mathbf{r}) &= b^{SPL}(\mathbf{r}) \\ c^{SPL1}(\mathbf{r}) &= \\ &\frac{(w_0(\mathbf{r}) - w_1(\mathbf{r}))(w_0(\mathbf{r}) + w_1(\mathbf{r}) - 2w_\infty(\mathbf{r}))}{(w_1(\mathbf{r}) - w_\infty(\mathbf{r}))^2} \end{aligned} \tag{36}$$

From the integral end points of eq 9, we expect $w_0(\mathbf{r})$ and $w_1(\mathbf{r})$ to play more important roles in the SPL1 interpolation scheme than the corresponding $w_\infty(\mathbf{r})$ quantity. However, if we only use $w_0(\mathbf{r})$ and $w_1(\mathbf{r})$ quantities, we do not have much flexibility, as we can only perform a linear interpolation between these two λ points:[40]

$$w_\lambda^{lin}(\mathbf{r}) \approx (w_1(\mathbf{r}) - w_0(\mathbf{r}))\lambda + w_0(\mathbf{r}) \tag{37}$$

DOI: 10.1021/acs.jctc.9b00129
J. Chem. Theory Comput. 2019, 15, 3580−3590

To better understand the role of $w_\infty(\mathbf{r})$ in the local SPL1 interpolation scheme, in Figure 5 we compare the correlation

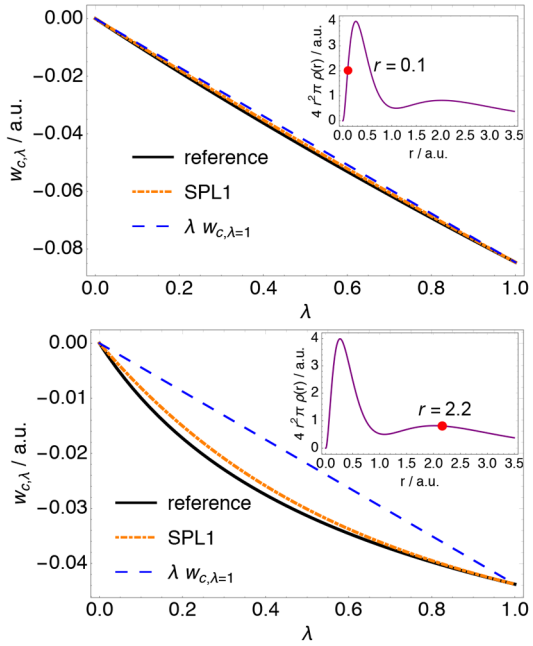

Figure 5. Reference and interpolated local correlation AC curves, $w_{c,\lambda}(\mathbf{r})$ of eq 8, for the Be atom with the reference electron placed at r = 0.1 au (upper panel) and r = 2.2 au (lower panel). (insets) positions of reference electrons in plots with the radial density of the Be atom.

component of the highly accurate local AC curves ($w_{c,\lambda}$) for the beryllium atom with those obtained by linear interpolation (eq 37) and SPL1 (eqs 34 and 36). In the upper panel of this figure, we place a reference electron in the core region (r = 0.2 au), while in the lower panel we place it in the valence region (r = 2.2 au). The highly accurate local AC curves have been taken from refs 19 and 45, and their computational details are the same as those of section 4. We can first notice the difference in the shape between the two AC curves: while in the core region the local AC curve is strongly linear in λ (a region dominated by dynamical correlation), the curvature of the local AC curve in the valence region is highly pronounced, mirroring a higher contribution of static correlation in this region.[22,45] For this reason, the linearly interpolated curve is in a fair agreement with the exact one in the core region, while it poorly models the AC curve in the valence region. On the other hand, the SPL1 interpolated local AC curves are in a good agreement with both of the exact local AC curves. From this simple example, we can already see that the use of $w_\infty(\mathbf{r})$ is able to provide more flexibility in an interpolation scheme when used in tandem with $w_0(\mathbf{r})$ and $w_1(\mathbf{r})$.

Upon using the SPL1 interpolation for the construction of the $T_c[\rho]$ component of the correlation energy, we can expect two sources of errors: one due to the interpolation itself and the other due to the inexactness of the $\mathbf{w}_{SPL1}(\mathbf{r})$ ingredients if approximations for their evaluation are used. Following the ideas of ref 19, in this section we disentangle these two sources of errors and isolate the error that is only due to the interpolation by using highly accurate energy densities forming $\mathbf{w}_{SPL1}(\mathbf{r})$. As the first step in assessing the accuracy of the SPL1 functional, in Table 1 we show the $T_c[\rho]$ values obtained by the SPL1 interpolation schemes for a set of small atoms (ions)

Table 1. Atomic (Ionic) Kinetic Component of Correlation Energies ($T_c[\rho]$) in Hartree Atomic Units Obtained by the Global and Local SPL1 Interpolations[a]

atom	T_c^{ref}	linear	global SPL1	local SPL1
H^-	0.0278	0.0343	0.0266	0.0263
He	0.0355	0.0378	0.0345	0.0344
Be	0.0700	0.0810	0.0758	0.0674
Ne^{6+}	0.1252	0.1543	0.1480	0.1305
Ne	0.2818	0.3145	0.3015	0.2980
Ar	0.3243	0.3641	0.3578	0.3424
MAE (mH)		20.23	14.00	7.46

[a] $T_c[\rho]$ energies obtained by the linear interpolation ($T_c[\rho] = -\frac{1}{2}U_c[\rho]$) are also shown for comparison.

that have been also considered in ref 22. The reference kinetic component of the correlation energy: $T_c[\rho] = \langle\Psi_1[\rho]|\hat{T}|\Psi_1[\rho]\rangle - \langle\Phi[\rho]|\hat{T}|\Phi[\rho]\rangle$ and the employed energy densities $w_0(\mathbf{r})$ and $w_1(\mathbf{r})$ have been taken from ref 22, and they have been computed at the CCSD/uncontracted-aug-cc-pCVTZ level of theory by using the Lieb maximization algorithm. The xc energy density from the strong coupling limit, $w_\infty(\mathbf{r})$, has been computed from eq 13 (see ref 13 for more details) on the density arising from the same level of theory. In addition to the local SPL1 model, $T_c[\rho]$ values in Table 1 have also been obtained by the global SPL1 scheme, which uses the same interpolation form (eqs 34 and 36), but with global ($W_0[\rho]$, $W_1[\rho]$, and $W_\infty[\rho]$) input quantities instead. For comparison, we also show the $T_c[\rho]$ values obtained by the linear interpolation (from eq 37, which yields $T_c[\rho] \approx -\frac{1}{2}U_c[\rho]$). We can see from Table 1 that in the case of all considered atoms/ions, both global and local SPL1 interpolations give more accurate $T_c[\rho]$ values than the linear interpolation of eq 37. In fact, an MAE of the local SPL1 interpolation is nearly 3 times smaller than that of the linear interpolation. As observed for other interpolation schemes,[22] the local variant of SPL is more accurate than its global counterpart (an MAE of the former interpolation is nearly by the factor of 2 smaller than that of the latter). For the same set of atoms/ions, the errors in total correlation energy made by the global and local SPL interpolations (eqs 34 and 35), assessed in ref 22, are more by the factor of 2 larger than the errors of their SPL1 variants. Nevertheless, we need to keep in mind that the higher accuracy of the SPL1 interpolations over the SPL ones is what one would expect, given that for the time being we use the exact information at λ = 1 in the SPL1 scheme. For this reason, the total error in $E_c[\rho]$ made by this interpolation scheme is equal to its error in $T_c[\rho]$.

Even more interesting than the global $T_c[\rho]$ values, we also analyze its local counterpart:

$$t_c^{hole}(\mathbf{r}) = \bar{w}_c(\mathbf{r}) - w_{c,\lambda=1}(\mathbf{r}) \tag{38}$$

This quantity represents the kinetic correlation energy density defined in terms of the differences in the electrostatic potentials between the λ-averaged xc hole and that at λ = 1 (see eqs 4 and 12). Even though this definition of the kinetic correlation energy density is not unique (see refs 60−62 for other definitions), we stay gauge consistent, in the sense that all energy density components throughout this work arise from the definition of $w_\lambda(\mathbf{r})$ of eq 4. In Figure 6, we show the highly accurate $t_c^{hole}(\mathbf{r})$ quantities together with those obtained by the SPL1 local interpolation and linear interpolation for the

DOI: 10.1021/acs.jctc.9b00129
J. Chem. Theory Comput. 2019, 15, 3580−3590

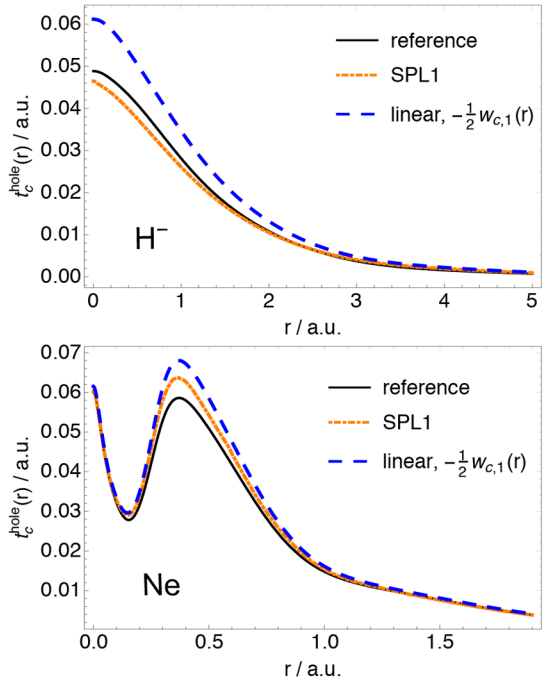

Figure 6. Reference and interpolated kinetic correlation energy densities in the gauge of the correlation hole (see eq 38) for the hydride ion (upper panel) and neon atom (lower panel).

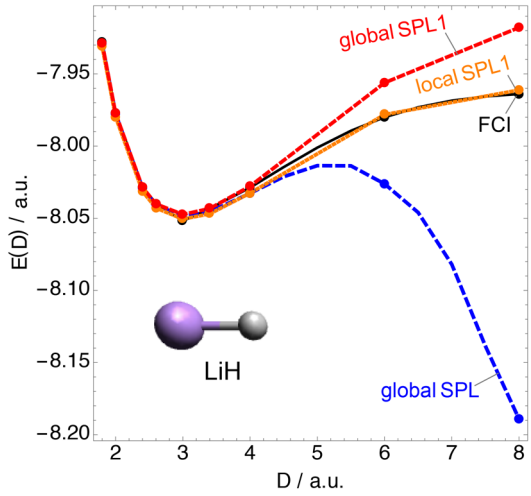

Figure 7. LiH dissociation curves obtained by the global SPL1, local SPL1, and global SPL AC-based interpolation schemes. The FCI curve, as a reference, is shown for comparison.

hydride ion and neon atom. As it can be seen from Figure 6, $t_c^{hole}(\mathbf{r})$ obtained by the SPL1 interpolation is in both cases more accurate than that obtained by the linear interpolation by using eq 37 (note that eq 37 yields $t_c^{hole} \approx -\frac{1}{2}w_{c,1}$). However, one can see that the improvement of the SPL1 interpolation over the simple linear one is more noticeable in the case of the hydride ion. This is due to the fact that $w_\lambda(\mathbf{r})$ is more linear in λ in the case of Ne than in the case of H^-. Furthermore, $t_c^{hole}(\mathbf{r})$ of the neon atom reflects its shell structure, and we can also see that the linearly interpolated $t_c^{hole}(\mathbf{r})$ is in a fairer agreement with its exact counterpart in the first shell than in the second. This observation also reflects the stronger linear dependence of $w_\lambda(\mathbf{r})$ in λ in the first shell of Ne than in the second shell.[45] In the remainder of this section we will focus on the dissociation of LiH, an interesting paradigmatic case of strong correlation that we will use here to highlight the advantage of the local SPL1 interpolation scheme over other AC interpolation-based schemes.

The difficulties of AC-based functionals in correctly describing the dissociation of LiH have been carefully studied in ref 22. From ref 22, we take an accurate LiH dissociation curve and that obtained with the global SPL functional and compare them with curves obtained with the SPL1 functional developed in the present work (in its both local and global variant). The plots of LiH dissociation curves are summarized in Figure 7. The reference curve has been obtained at the full-CI within the uncontracted cc-pVDZ basis set and the quantities for the SPL interpolation had been obtained at the same level of theory by using the Lieb maximization algorithm. The $w_1(\mathbf{r})$ energy density and its global counterpart ($W_1[\rho]$) used in the SPL1 interpolation schemes have been computed from $\Psi_{\lambda=1}[\rho]$ also at the full-CI/uncontracted-cc-pVDZ level of theory by using the GAMESS-US package.[31] While for atoms we used the exact form of $w_\infty(\mathbf{r})$, for LiH we could not reach the convergence level with the algorithm of ref 16 that will produce highly accurate $w_\infty(\mathbf{r})$. For this reason, for LiH we have used an accurate approximation to this quantity from the *nonlocal radius* (NLR) model.[63]

Before analyzing Figure 7, we remember that the dissociation of LiH is accompanied by the KS HOMO−LUMO gap closing, as the bond stretches, and the consequent divergence of the corresponding global AC initial slope: $W_0'[\rho] \to -\infty$.[22,64] The local variant of the (exact) initial AC slope also diverges in this case: $w_0'(\mathbf{r}) \to -\infty$,[22] as the KS HOMO−LUMO energy gap also appears in the denominator for the $w_0'(\mathbf{r})$ expression.[19] As the result of the two divergences, the approximate xc functional from both local and global SPL interpolation schemes will tend to $E_{xc}^{SPL}[\rho] \to W_\infty[\rho]$, as the bond stretches. For one-electron-like systems this is still fine; as for these systems, $E_{xc}[\rho] = W_\infty[\rho]$ holds. However, for general systems, electrons at the infinite coupling strength are overcorrelated, and thus, $W_\infty[\rho]$ is much lower than the exact $E_{xc}[\rho]$ functional. For this reason, a scenario in which $E_{xc}^{SPL}[\rho]$ approaches $W_\infty[\rho]$, as the bond stretches, leads to the *overcorrelation error*. Due to this error, the LiH dissociation curve of Figure 7 obtained with the global SPL unphysically *bends down* at large bond lengths, with unacceptably low total energies. The overcorrelation error is avoided within both global and local SPL1 interpolation scheme, as they do not make use of the initial AC slope (eqs 34 and 36). Despite this, as it can be seen from Figure 7, the dissociation curve from the global SPL1 is above the exact curve at large bond lengths, due to the size-consistency error. Contrary to the SPL models and the global SPL1 model, both size consistency and over-correlation error are absent in the local SPL1 model. As it can be seen from Figure 7, the dissociation curve from the local SPL1 model is in a fair agreement with the exact curve.

We again remind the reader that the use of the highly accurate and thus expensive ingredients enabled us to isolate and assess the error of the AC models that is only due to the interpolation. This interpolation error reduces to the over-correlation error (in the local and global SPL scheme) and the size-consistency error (in the case of the global SPL and global SPL1 scheme). Given that these errors are absent in the local SPL1 scheme, our findings support the use of this scheme for

DOI: 10.1021/acs.jctc.9b00129
J. Chem. Theory Comput. 2019, 15, 3580−3590

the construction of future approximations for the kinetic correlation energy. For any practical purposes, in place of the exact and computationally intractable $w_1(\mathbf{r})$ quantity, its approximations need to be used. First of all, this would include the approximate $w_1(\mathbf{r})$ from the MRF model improved by the incorporation of the constraint given by eq 32 but also other suitable approximations that can be used for building $w_1(\mathbf{r})$.[44,50,51]

6. CONCLUSIONS AND PERSPECTIVES

In the present paper we study different features of the MRF functional to lay the foundation for the development of new DFAs based on it. We use highly accurate energy densities of small atoms to reveal the structure of the exact MRF objects. We also use the crucial MRF physical quantity, the charge associated with effective distance between electrons, to analyze other approximate xc energy densities in the *gauge* given by eq 4. By developing the MRF reverse machinery in section 4, we pave the way for the construction of the MRF xc functional on top of exact exchange (eq 31). We also use this reverse machinery to define a simple constraint which forces the MRF xc energy density at the full coupling strength to lie below that of the exact exchange, a feature that is presently missed by the MRF xc energy densities arising from eq 19.

We also develop a local interpolation along the adiabatic connection-based scheme (called SPL1) used for the construction of the approximate $T_c[\rho]$ functional, and we obtain it by combining the information from the weakly, strongly and physically interacting regimes. We show that, unlike other AC interpolation-based methods, the SPL1 method does not suffer from the overcorrelation and size-consistency errors upon stretching bonds of systems that dissociate into open-shell fragments. As the first step in assessing the accuracy of the SPL1 scheme, we disentangle its sources of errors and isolate the error that is only due to the interpolation. Our tests on small atoms/ions and LiH molecule show that the SPL1 scheme recovers the $T_c[\rho]$ energy rather accurately. In future work we will use the SPL1 approach in tandem with the MRF xc energy densities at $\lambda = 1$ (e.g., those that would arise from forms akin to eq 19, improved by the insights obtained from the exact results in sections 3.1 and 4).

Our ongoing efforts to implement the MRF functional into quantum-chemical software are based on the recent work of Bahman et al., who showed how $N_e(\mathbf{r}, u)$ of eq 16, as the key MRF ingredient, can be efficiently calculated by using a Gaussian basis set.[55] The idea is to have a flexible implementation, so that new and improved forms of the fluctuation functions (see e.g., eqs 21 and 19), resulting from the findings of the present work, can be easily assessed. In future work we will also make use of the direct transferability of the MRF framework to other isotropic interactions between particles (e.g., short- and long-range components of the Coulomb interaction). This, in turn, we will allow us to use the range separation techniques[65] to further tune the accuracy of the MRF functional.

APPENDIX A: LDA AND BECKE-ROUSSEL ENERGY DENSITIES

The LDA xc energy density at the full coupling strength used in section 3.2 is obtained from[66]

$$w_1^{\mathrm{LDA}}(r_s) = \frac{1}{r_s}\frac{\partial}{\partial r_s}(r_s^2 \epsilon_{xc}(r_s)) \tag{39}$$

where $r_s(\mathbf{r})$ is the Wigner–Seitz radius: $r_s(\mathbf{r}) = \left(\frac{4}{3}\pi\rho(\mathbf{r})\right)^{-1/3}$ and $\epsilon_{xc}(r_s)$ is the LDA (λ-averaged) xc energy density. We have used the PW92 functional for computing the correlation part of $\epsilon_{xc}(r_s)$.[67]

Section 3.2 also employs the approximate energy density from the Becke-Roussel (BR) exchange hole model.[35] This model hole takes the following form:

$$h_{x,\sigma}^{\mathrm{BR}}(\mathbf{r}, u) = \frac{a_\sigma^{\mathrm{BR}}}{16\pi b_\sigma^{\mathrm{BR}} u}[(a_\sigma^{\mathrm{BR}}|b_\sigma^{\mathrm{BR}} - u| + 1)e^{-a_\sigma^{\mathrm{BR}}|b_\sigma^{\mathrm{BR}}-u|} - (a_\sigma^{\mathrm{BR}}|b_\sigma^{\mathrm{BR}} + u| + 1)e^{-a_\sigma^{\mathrm{BR}}|b_\sigma^{\mathrm{BR}}+u|}] \tag{40}$$

where the $a_\sigma^{\mathrm{BR}}(\mathbf{r})$ and $b_\sigma^{\mathrm{BR}}(\mathbf{r})$ are the parameters that are fixed by the exact on-top depth and curvature of the exchange-hole ($u \to 0$):[68]

$$h_{x,\sigma}(\mathbf{r}, u) = -\rho_\sigma(\mathbf{r}) - Q_\sigma(\mathbf{r})u^2 + O(u^4) \tag{41}$$

where $\rho_\sigma(\mathbf{r})$ is the density of spin-σ electrons. The $Q_\sigma(\mathbf{r})$ quantity is the exchange hole curvature given by

$$Q_\sigma(\mathbf{r}) = \frac{1}{6}\left[\nabla^2\rho_\sigma(\mathbf{r}) - 4\tau_\sigma(\mathbf{r}) - \frac{1}{2}\frac{|\nabla\rho_\sigma(\mathbf{r})|^2}{\rho_\sigma(\mathbf{r})}\right] \tag{42}$$

where $\tau_\sigma(\mathbf{r}) = \sum_i^{\mathrm{occ}}|\nabla\phi_{i,\sigma}(\mathbf{r})|^2$, with $\phi_{i,\sigma}(\mathbf{r})$ being the occupied KS orbitals. The $a_\sigma^{\mathrm{BR}}(\mathbf{r})$ and $b_\sigma^{\mathrm{BR}}(\mathbf{r})$ parameters can be obtained by solving a simple 1D nonlinear equation for every $\mathbf{r}$ gridpoint (see refs 43 and 69 for more details). Then, the underlying energy density, $w_x^{\mathrm{BR}}(\mathbf{r})$, is obtained by plugging eq 40 into eq 4, and it has the following analytic form:

$$w_{x,\sigma}^{\mathrm{BR}}(\mathbf{r}) = -\frac{1 - e^{-y_\sigma(\mathbf{r})} - \frac{1}{2}y_\sigma(\mathbf{r})e^{-y_\sigma(\mathbf{r})}}{2b^{\mathrm{BR}}(\mathbf{r})} \tag{43}$$

where $y_\sigma(\mathbf{r}) = a_\sigma^{\mathrm{BR}}(\mathbf{r})b_\sigma^{\mathrm{BR}}(\mathbf{r})$. Since in this work we calculate $w_{x,\sigma}^{\mathrm{BR}}(\mathbf{r})$ only for closed-shell species (He and H^-), we have that $w_x^{\mathrm{BR}}(\mathbf{r}) = w_{x,\alpha}^{\mathrm{BR}}(\mathbf{r}) = w_{x,\beta}^{\mathrm{BR}}(\mathbf{r})$. The densities used for the evaluation of the LDA and BR xc energy densities have been obtained at the FCI/aug-cc-pVQZ level, like all the other densities employed in section 3.

AUTHOR INFORMATION

Corresponding Author

*E-mail: svuckovi@uci.edu.

ORCID

Stefan Vuckovic: 0000-0002-0768-9176

Notes

The author declares no competing financial interest.

ACKNOWLEDGMENTS

The author thanks T. J. P. Irons and A. M. Teale for the λ-dependent energy densities data used in sections 3 and 4, and P. Gori-Giorgi for a critical reading of the manuscript. This work is part of the research programme Rubicon with project number 019.181EN.026, which is financed by The Netherlands Organization for Scientific Research (NWO). The author also acknowledges financial support from the European Research Council under H2020/ERC Consolidator Grant corr-DFT (Grant No. 648932).

DOI: 10.1021/acs.jctc.9b00129
J. Chem. Theory Comput. 2019, 15, 3580−3590

REFERENCES

(1) Kohn, W.; Sham, L. J. Self-consistent equations including exchange and correlation effects. *Phys. Rev.* **1965**, *140*, A1133.
(2) Cohen, A. J.; Mori-Sánchez, P.; Yang, W. Challenges for density functional theory. *Chem. Rev.* **2012**, *112*, 289.
(3) Becke, A. D. Perspective: Fifty years of density-functional theory in chemical physics. *J. Chem. Phys.* **2014**, *140*, 18A301.
(4) Pribram-Jones, A.; Gross, D. A.; Burke, K. Dft: A theory full of holes? *Annu. Rev. Phys. Chem.* **2015**, *66*, 283−304.
(5) Perdew, J. P.; Schmidt, K. Jacob's ladder of density functional approximations for the exchange-correlation energy. *AIP Conference Proceedings*, 2001; pp 1−20.
(6) Staroverov, V. N.; Scuseria, G. E.; Tao, J.; Perdew, J. P. Tests of a ladder of density functionals for bulk solids and surfaces. *Phys. Rev. B: Condens. Matter Mater. Phys.* **2004**, *69*, 075102.
(7) Perdew, J. P.; Ruzsinszky, A.; Tao, J.; Staroverov, V. N.; Scuseria, G. E.; Csonka, G. I. Prescription for the design and selection of density functional approximations: More constraint satisfaction with fewer fits. *J. Chem. Phys.* **2005**, *123*, 062201.
(8) Mardirossian, N.; Head-Gordon, M. Thirty years of density functional theory in computational chemistry: an overview and extensive assessment of 200 density functionals. *Mol. Phys.* **2017**, *115*, 2315−2372.
(9) Cohen, A. J.; Mori-Sanchez, P.; Yang, W. Insights into current limitations of density functional theory. *Science* **2008**, *321*, 792.
(10) Seidl, M. Strong-interaction limit of density-functional theory. *Phys. Rev. A: At., Mol., Opt. Phys.* **1999**, *60*, 4387.
(11) Seidl, M.; Perdew, J. P.; Levy, M. Strictly correlated electrons in density-functional theory. *Phys. Rev. A: At., Mol., Opt. Phys.* **1999**, *59*, 51.
(12) Seidl, M.; Perdew, J. P.; Kurth, S. Simulation of all-order density-functional perturbation theory, using the second order and the strong-correlation limit. *Phys. Rev. Lett.* **2000**, *84*, 5070.
(13) Seidl, M.; Gori-Giorgi, P.; Savin, A. Strictly correlated electrons in density-functional theory: A general formulation with applications to spherical densities. *Phys. Rev. A: At., Mol., Opt. Phys.* **2007**, *75*, 042511.
(14) Gori-Giorgi, P.; Vignale, G.; Seidl, M. Electronic zero-point oscillations in the strong-interaction limit of density functional theory. *J. Chem. Theory Comput.* **2009**, *5*, 743−753.
(15) Gori-Giorgi, P.; Seidl, M.; Vignale, G. Density-functional theory for strongly interacting electrons. *Phys. Rev. Lett.* **2009**, *103*, 166402.
(16) Vuckovic, S.; Wagner, L. O.; Mirtschink, A.; Gori-Giorgi, P. Hydrogen Molecule Dissociation Curve with Functionals Based on the Strictly Correlated Regime. *J. Chem. Theory Comput.* **2015**, *11*, 3153−3162.
(17) Vuckovic, S.; Gori-Giorgi, P. Simple fully non-local density functionals for the electronic repulsion energy. *J. Phys. Chem. Lett.* **2017**, *8*, 2799−2805.
(18) Burke, K.; Cruz, F. G.; Lam, K.-C. Unambiguous exchange-correlation energy density. *J. Chem. Phys.* **1998**, *109*, 8161−8167.
(19) Vuckovic, S.; Irons, T. J.; Savin, A.; Teale, A. M.; Gori-Giorgi, P. Exchange-correlation functionals via local interpolation along the adiabatic connection. *J. Chem. Theory Comput.* **2016**, *12*, 2598−2610.
(20) Langreth, D. C.; Perdew, J. P. The exchange-correlation energy of a metallic surface. *Solid State Commun.* **1975**, *17*, 1425−1429.
(21) Gunnarsson, O.; Lundqvist, B. I. Exchange and correlation in atoms, molecules, and solids by the spin-density-functional formalism. *Phys. Rev. B* **1976**, *13*, 4274.
(22) Vuckovic, S.; Irons, T. J. P.; Wagner, L. O.; Teale, A. M.; Gori-Giorgi, P. Interpolated energy densities, correlation indicators and lower bounds from approximations to the strong coupling limit of DFT. *Phys. Chem. Chem. Phys.* **2017**, *19*, 6169−6183.
(23) Cruz, F. G.; Lam, K.-C.; Burke, K. Exchange- Correlation Energy Density from Virial Theorem. *J. Phys. Chem. A* **1998**, *102*, 4911−4917.
(24) Vuckovic, S.; Levy, M.; Gori-Giorgi, P. Augmented potential, energy densities, and virial relations in the weak-and strong-interaction limits of DFT. *J. Chem. Phys.* **2017**, *147*, 214107.
(25) Tao, J.; Staroverov, V. N.; Scuseria, G. E.; Perdew, J. P. Exact-exchange energy density in the gauge of a semilocal density-functional approximation. *Phys. Rev. A: At., Mol., Opt. Phys.* **2008**, *77*, 012509.
(26) Mirtschink, A.; Seidl, M.; Gori-Giorgi, P. Energy densities in the strong-interaction limit of density functional theory. *J. Chem. Theory Comput.* **2012**, *8*, 3097−3107.
(27) Gori-Giorgi, P.; Seidl, M. Density functional theory for strongly-interacting electrons: perspectives for physics and chemistry. *Phys. Chem. Chem. Phys.* **2010**, *12*, 14405−14419.
(28) Mendl, C. B.; Lin, L. Kantorovich dual solution for strictly correlated electrons in atoms and molecules. *Phys. Rev. B: Condens. Matter Mater. Phys.* **2013**, *87*, 125106.
(29) Vuckovic, S. Fully Nonlocal Exchange-Correlation Functionals from the Strong-coupling limit of Density Functional Theory. Ph.D. thesis, Vrije Universiteit Amsterdam, The Netherlands, 2017.
(30) Teale, A.; Coriani, S.; Helgaker, T. The calculation of adiabatic-connection curves from full configuration-interaction densities: Two-electron systems. *J. Chem. Phys.* **2009**, *130*, 104111.
(31) Ishimura, K.; Acc, S. N. T. C.; McMurchie, L.; Davidson, E.; Rys, J. General Atomic and Molecular Electronic Structure System. *J. Comput. Chem.* **1993**, *14*, 1347−1363.
(32) Dunning, T. H. Gaussian basis sets for use in correlated molecular calculations. I. The atoms boron through neon and hydrogen. *J. Chem. Phys.* **1989**, *90*, 1007.
(33) Görling, A.; Levy, M. Correlation-energy functional and its high-density limit obtained from a coupling-constant perturbation expansion. *Phys. Rev. B: Condens. Matter Mater. Phys.* **1993**, *47*, 13105.
(34) Görling, A.; Levy, M. Exact Kohn-Sham scheme based on perturbation theory. *Phys. Rev. A: At., Mol., Opt. Phys.* **1994**, *50*, 196.
(35) Becke, A.; Roussel, M. Exchange holes in inhomogeneous systems: A coordinate-space model. *Phys. Rev. A: At., Mol., Opt. Phys.* **1989**, *39*, 3761.
(36) Burke, K.; Cruz, F. G.; Lam, K.-C. Unambiguous exchange-correlation energy density. *J. Chem. Phys.* **1998**, *109*, 8161−8167.
(37) Gunnarsson, O.; Lundqvist, B.; Wilkins, J. Contribution to the cohesive energy of simple metals: Spin-dependent effect. *Phys. Rev. B* **1974**, *10*, 1319.
(38) Gunnarsson, O.; Jonson, M.; Lundqvist, B. I. Descriptions of exchange and correlation effects in inhomogeneons electron systems. *Phys. Rev. B: Condens. Matter Mater. Phys.* **1979**, *20*, 3136.
(39) Clementi, E.; Chakravorty, S. J. A comparative study of density functional models to estimate molecular atomization energies. *J. Chem. Phys.* **1990**, *93*, 2591−2602.
(40) Becke, A. D. A new mixing of Hartree-Fock and local density-functional theories. *J. Chem. Phys.* **1993**, *98*, 1372.
(41) Perdew, J. P.; Staroverov, V. N.; Tao, J.; Scuseria, G. E. Density functional with full exact exchange, balanced nonlocality of correlation, and constraint satisfaction. *Phys. Rev. A: At., Mol., Opt. Phys.* **2008**, *78*, 052513.
(42) Becke, A. D. A real-space model of nondynamical correlation. *J. Chem. Phys.* **2003**, *119*, 2972−2977.
(43) Becke, A. D.; Johnson, E. R. A unified density-functional treatment of dynamical, nondynamical, and dispersion correlations. *J. Chem. Phys.* **2007**, *127*, 124108.
(44) Becke, A. D. Density functionals for static, dynamical, and strong correlation. *J. Chem. Phys.* **2013**, *138*, 074109.
(45) Irons, T. J.; Teale, A. M. The coupling constant averaged exchange-correlation energy density. *Mol. Phys.* **2015**, *114*, 484−497.
(46) Purvis, G. D.; Bartlett, R. J. A full coupled-cluster singles and doubles model: The inclusion of disconnected triples. *J. Chem. Phys.* **1982**, *76*, 1910−1918.
(47) Wu, Q.; Yang, W. A direct optimization method for calculating density functionals and exchange-correlation potentials from electron densities. *J. Chem. Phys.* **2003**, *118*, 2498−2509.
(48) Teale, A.; Coriani, S.; Helgaker, T. Accurate calculation and modeling of the adiabatic connection in density functional theory. *J. Chem. Phys.* **2010**, *132*, 164115.

DOI: 10.1021/acs.jctc.9b00129
J. Chem. Theory Comput. 2019, 15, 3580−3590

(49) Van Leeuwen, R. Kohn-Sham potentials in density functional theory. Ph.D. thesis, Vrije Universiteit Amsterdam, The Netherlands, 1994.
(50) Kong, J.; Proynov, E. Density Functional Model for Nondynamic and Strong Correlation. *J. Chem. Theory Comput.* **2016**, *12*, 133−143.
(51) Pavlíková Přecechtělová, J.; Bahmann, H.; Kaupp, M.; Ernzerhof, M. Design of exchange-correlation functionals through the correlation factor approach. *J. Chem. Phys.* **2015**, *143*, 144102.
(52) Precechtelová, J.; Bahmann, H.; Kaupp, M.; Ernzerhof, M. Communication: A non-empirical correlation factor model for the exchange-correlation energy. *J. Chem. Phys.* **2014**, *141*, 111102.
(53) Ernzerhof, M. Construction of the adiabatic connection. *Chem. Phys. Lett.* **1996**, *263*, 499.
(54) Zhou, Y.; Bahmann, H.; Ernzerhof, M. Construction of exchange-correlation functionals through interpolation between the non-interacting and the strong-correlation limit. *J. Chem. Phys.* **2015**, *143*, 124103.
(55) Bahmann, H.; Zhou, Y.; Ernzerhof, M. The shell model for the exchange-correlation hole in the strong-correlation limit. *J. Chem. Phys.* **2016**, *145*, 124104.
(56) Seidl, M. Adiabatic connection in density-functional theory: Two electrons on the surface of a sphere. *Phys. Rev. A: At., Mol., Opt. Phys.* **2007**, *75*, 062506.
(57) Seidl, M.; Perdew, J. P.; Kurth, S. Density functionals for the strong-interaction limit. *Phys. Rev. A: At., Mol., Opt. Phys.* **2000**, *62*, 012502.
(58) Fabiano, E.; Gori-Giorgi, P.; Seidl, M.; Della Sala, F. Interaction-Strength Interpolation Method for Main-Group Chemistry: Benchmarking, Limitations, and Perspectives. *J. Chem. Theory Comput.* **2016**, *12*, 4885−4896.
(59) Kong, J.; Proynov, E. Density Functional Model for Nondynamic and Strong Correlation. *J. Chem. Theory Comput.* **2016**, *12*, 133−143.
(60) Buijse, M. A.; Baerends, E. J.; Snijders, J. G. Analysis of correlation in terms of exact local potentials: Applications to two-electron systems. *Phys. Rev. A: At., Mol., Opt. Phys.* **1989**, *40*, 4190.
(61) Gritsenko, O. V.; Leeuwen, R. v.; Baerends, E. J. Molecular exchange-correlation Kohn-Sham potential and energy density from ab initio first-and second-order density matrices: Examples for XH (X= Li, B, F). *J. Chem. Phys.* **1996**, *104*, 8535−8545.
(62) Giarrusso, S.; Vuckovic, S.; Gori-Giorgi, P. Response potential in the strong-interaction limit of DFT: Analysis and comparison with the coupling-constant average. *J. Chem. Theory Comput.* **2018**, *14*, 4151.
(63) Wagner, L. O.; Gori-Giorgi, P. Electron avoidance: A nonlocal radius for strong correlation. *Phys. Rev. A: At., Mol., Opt. Phys.* **2014**, *90*, 052512.
(64) Gritsenko, O. V.; Baerends, E. J. Effect of molecular dissociation on the exchange-correlation Kohn-Sham potential. *Phys. Rev. A: At., Mol., Opt. Phys.* **1996**, *54*, 1957.
(65) Savin, A. In *Recent Developments of Modern Density Functional Theory*; Seminario, J. M., Ed.; Elsevier: Amsterdam, 1996; pp 327−357.
(66) March, N. Kinetic and potential energies of an electron gas. *Phys. Rev.* **1958**, *110*, 604.
(67) Perdew, J. P.; Wang, Y. Accurate and simple analytic representation of the electron-gas correlation energy. *Phys. Rev. B: Condens. Matter Mater. Phys.* **1992**, *45*, 13244.
(68) Becke, A. Hartree-Fock exchange energy of an inhomogeneous electron gas. *Int. J. Quantum Chem.* **1983**, *23*, 1915−1922.
(69) Proynov, E.; Gan, Z.; Kong, J. Analytical representation of the Becke-Roussel exchange functional. *Chem. Phys. Lett.* **2008**, *455*, 103−109.

DOI: 10.1021/acs.jctc.9b00129
J. Chem. Theory Comput. 2019, 15, 3580−3590